PRAMANA
— journal of
physics

Vol. 70, No. 6
June 2008
pp. 989–1007

Numerical simulations in granular matter: The discharge of a 2D silo

GABRIEL PÉREZ
Departamento de Física Aplicada, Centro de Investigación y de Estudios Avanzados, del Instituto Politécnico Nacional, Unidad Mérida, Apartado Postal 73 "Cordemex", 97310 Mérida, Yucatán, México
E-mail: gperez@mda.cinvestav.mx; ermenegildito@yahoo.com.mx

Abstract. In this paper I give a short and elementary review of numerical simulations in granular assemblies, giving the process of discharge of a 2D silo as an example. The strengths and limitations of different approaches are discussed, together with some comments on the specific issues related to the numerics of discontinuous dissipative collisions.

Keywords. Granular media; numerical simulations.

PACS Nos 45.70.-n; 45.70.Ht; 05.70.Jk

1. Introduction

Granular matter is defined as the collection of independent pieces of solid matter with sizes ranging from hundreds of μm to several km, which interact with each other only by excluded volume and are too large to be disturbed by thermal fluctuations [1–4]. This form of matter, although very common in nature – think of sand, gravel, edible grains, metal nuggets, the asteroid belt, etc. – and of great practical importance, has been explored by physicists only recently. The main reason for this is that the collisions between different elements of the assembly – in short, different grains – are dissipative, and therefore not amenable to a Hamiltonian description. This implies that all the well-known techniques of statistical mechanics do not apply, and that granular matter is either static or out of equilibrium.

There is plenty of interesting phenomenology in both cases. In the static situation one finds that, due to the macroscopic size of the constituents and to quenched disorder in their packing arrangement, granular matter does not show homogeneous distributions of stresses, and tend to form arches that direct the load of the material sideways [5]. As a consequence of this, pressure inside a container saturates (Janssen's law [6]) and systems can spontaneously stop flowing (jamming) [7].

In the dynamic case, the most notorious effects are directly related to being out of equilibrium, as already mentioned. In particular, it is common that driven inhomogeneous granular assemblies segregate by size, weight, or even by frictional

characteristics [8–11], reducing in the process the entropy of the aggregate; in homogeneous assemblies clustering [12–14] – usually called 'inhomogeneous cooling' – is often found.

There is no general theoretical framework to describe granular matter, and most of the analytical approaches are limited to diluted assemblies in the low dissipative limit [15]. Therefore our understanding of the experimental results come either from ad hoc models, applicable to very specific experimental settings, and from numerical simulations. These represent a particular version of the well-known methods of molecular dynamics (MD) [16,17], adapted to discontinuous potentials and dissipation.

In this paper I want to give a limited, but hopefully pedagogical, view of some of the issues confronted in these simulations, together with the results of a particular application, namely, the flow of matter out of a 2D silo. The text is directed mostly to researchers in the nonlinear community with limited experience in MD, and so it remains very close to the basics. In §2, we will discuss the general issues of granular matter simulation, in §3 we will concentrate on the soft particle model (time-driven molecular dynamics), in §4 will describe the silo model and the results of a soft particle simulation, and some final comments will be given in §5.

2. Numerical approaches

There are basically three main ways of doing a simulation in granular matter, depending on (a) whether one takes the grains to be absolutely hard or not, and (b) whether one allows long-lasting contacts – going all the way to static assemblies – or limit these contact to be instantaneous. The first approach, known as *event driven molecular dynamics* (EDMD), goes back to the pioneering work of Adler and Wainwright in the hard disk gas [18], and considers a group of grains that move freely (or with some easily integrable kinematics) between collisions. Upon collision the velocities of the colliding grains are changed accordingly to some predetermined rules that preserve linear and angular momentum but reduce kinetic energies. For grains with spherical symmetry the rules are simple and are given in the following way [16,19,20]: consider a collision between two grains a and b, or radii R_a and R_b, masses m_a and m_b, and inertia moments I_a and I_b, located in positions $\mathbf{r}_a$ and $\mathbf{r}_b$ in 3D space, as shown in figure 1. Define the distance vector between the spheres, and the corresponding normal vector, as

$$\Delta\mathbf{r} \equiv \mathbf{r}_b - \mathbf{r}_a, \quad \hat{\mathbf{n}} = \Delta\mathbf{r}/|\Delta\mathbf{r}|. \tag{1}$$

Now, the relative velocity at the contact point is

$$\mathbf{v}_{ab} = \mathbf{v}_a - \mathbf{v}_b + (R_a\boldsymbol{\omega}_a + R_b\boldsymbol{\omega}_b) \times \hat{\mathbf{n}}, \tag{2}$$

where $\boldsymbol{\omega}_a$ and $\boldsymbol{\omega}_b$ are the respective angular velocities. Split this relative velocity into its normal and tangential components

$$\mathbf{v}_{ab}(n) = (\mathbf{v}_{ab} \cdot \hat{\mathbf{n}})\,\hat{\mathbf{n}}, \tag{3}$$

$$\mathbf{v}_{ab}(s) = \mathbf{v}_{ab} - \mathbf{v}_{ab}(n) = -\hat{\mathbf{n}} \times (\hat{\mathbf{n}} \times \mathbf{v}_{ab}). \tag{4}$$

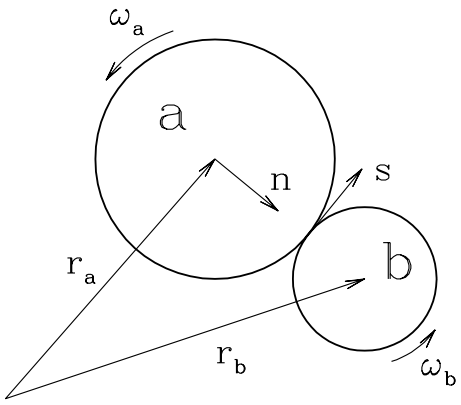

Figure 1. Diagram of a collision of two spherical grains.

Upon collision these two components of velocity transform as

$$\mathbf{v}'_{ab}(n) = -\epsilon_n \mathbf{v}_{ab}(n), \tag{5}$$

$$\mathbf{v}'_{ab}(s) = \epsilon_s \mathbf{v}_{ab}(s), \tag{6}$$

where ϵ_n and ϵ_s are the normal and tangential restitution coefficients, restricted to the ranges $0 \leq \epsilon_n \leq 1$ and $-1 \leq \epsilon_s \leq 1$. These represent the ratios of the normal and tangential velocities after the collision to the corresponding velocities before. The limits $|\epsilon| \to 1$ correspond to perfectly elastic collisions, while $|\epsilon| \to 0$ give the behavior in completely inelastic (fully dissipative) situation. Even though in many simulations the restitution coefficients are assumed as constants, they are in principle velocity dependent. In particular, care must be taken to let ϵ_n tend to 1 if very small velocities appear, in order to avoid the so-called 'inelastic collapse', where two grains forced to be close to each other have a divergent number of collisions as their relative velocity vanishes [21,22].

To complete the process conservation of linear and angular momenta around the contact point are used. Here it is convenient to introduce a few definitions: start by calling $\mathcal{I} \equiv I/mR^2$ the adimensional reduced inertia moment of a grain with spherical symmetry, and define a couple of constants

$$S = m_a + m_b, \qquad T = m_a \frac{1+\mathcal{I}_b}{\mathcal{I}_b} + m_b \frac{1+\mathcal{I}_a}{\mathcal{I}_a}. \tag{7}$$

Using these constants, and the restitution coefficients, define the vector

$$\mathbf{D} = -\frac{1+\epsilon_n}{S}\,\mathbf{v}_{ab}(n) + \frac{\epsilon_s - 1}{T}\,\mathbf{v}_{ab}(s); \tag{8}$$

using this vector all after-collision quantities can be calculated:

$$\mathbf{v}'_a = \mathbf{v}_a + m_b \mathbf{D}, \quad \boldsymbol{\omega}'_a = \boldsymbol{\omega}_a + \left(\frac{m_b}{R_a \mathcal{I}_a}\right) \hat{\mathbf{n}} \times \mathbf{D}, \tag{9}$$

$$\mathbf{v}'_b = \mathbf{v}_b - m_a \mathbf{D}, \quad \boldsymbol{\omega}'_b = \boldsymbol{\omega}_b + \left(\frac{m_a}{R_b \mathcal{I}_b}\right) \hat{\mathbf{n}} \times \mathbf{D}. \tag{10}$$

In its simplest form, the typical calculation in this scheme will go as follows: starting from some initial configuration of positions and velocities, at some time t_0, all future first collisions, either between two grains or between a grain and a wall, are analytically calculated. The times of these *events* are sorted and the first one, that happens at t_1, is realized. This means that all grains are moved to their calculated positions at t_1, and the linear and angular velocities of the grains participating in the collision are recalculated according to the given formulas. At this moment the collisions between the grains that changed their velocities and all other grains and walls are recalculated, and their timings are used to insert these new events in the sorted list. Finally, one has to remember that the change in velocities of the colliding grains mean that some previously calculated events are now not going to happen, and therefore should be deleted from the sorted list. After doing this, time advances to the next event on the list, and so on.

There are of course many improvements over this simplistic approach. A very useful one is the division of the physical space in small cells, containing just a few grains, so that the search for collision partners for a given grain is restricted to the next nearest cells. The price to be paid for this improvement is that one now needs to know in which cell each grain is, and this means considering the change of cell of any grain as an event, to be included in the list of future events. Another important algorithmic trick is to organize the event time-table not in the form of a simple list, but in the form of a binary tree. This accelerates the location of new events in the time-table, giving a computational effort of just $\log_2 N$ for N grains. It is also possible to assign a different time variable to each grain, so that one does not need to upgrade the variables of every grain in the assembly upon a collision, only of those that actually collided. Setting up a working code with all these subtleties is however not completely trivial; fortunately very detailed instructions on how to do this are given in refs [23–25].

The main advantage of EDMD is its speed. Simulations with tens of thousands of grains for many minutes of actual kinematics can be carried out in reasonable time even with modest desktop computers. There are however some important drawbacks: first of all, it is not possible to consider any static situation: in its very essence, the method assumes colliding grains and cannot deal with one grain just sitting on top of some others. This also means that very dense flows – say, the drainage of a silo – are not really well-handled by EDMD. Another fundamental problem is the inability of the method to incorporate any complex external potential: the trajectory of a grain has to be analytically solved between collisions, otherwise the advantages of this approach disappear. A minor point that is also missed by the method is the qualitative difference that exists between fluidized material, where most collisions are binary, and dense dynamics where multiple simultaneous interactions are common; this impossibility arises because EDMD can handle only binary collisions.

A second approach tries to follow the dynamics step by step, and at the same time to preserve the impenetrability of the grains. It is known as contact dynamics (CD), and allows for both collisions and standing contacts [26–29]. In order to do so, the method looks for a solution of the equations of motion using an implicit Euler method, where at every iteration positions, velocities and internal (contact) forces have to be calculated:

$$\mathbf{r}_i(t+\delta t) = \mathbf{r}_i(t) + \mathbf{v}_i(t+\Delta t)\,\Delta t, \tag{11}$$

$$\mathbf{v}_i(t+\delta t) = \mathbf{v}_i(t) + \frac{1}{m_i}\mathbf{F}_i(t+\Delta t)\,\Delta t - \hat{\mathbf{z}}g\,\Delta t, \tag{12}$$

where it has been assumed that the only external force is gravity. Given that no *a priori* internal forces are prescribed, the method imposes two conditions: the first says that the normal force between two grains is zero when they are not in touch, and it is whatever is needed to avoid interpenetration when they touch. This is known as the Signorini condition. For tangential forces, arising from friction, the method implements exactly the Coulomb form: if the sum of other tangential forces has a magnitude below the limit $\mu_s N$ (here N is the normal force), static friction will provide a counter-force of equal magnitude and opposite direction, so that the contact point does not slide; otherwise a dynamic friction of the form $-\mu_d N\hat{\mathbf{v}}_t$ appears. Now, the main difficulty here is that as one is trying to simultaneously solve for the future values of position and velocity, and for the forces that depend on them, for more than two particles, the resulting equations of motion have to be solved in a self-consistent manner. Thus, every step of integration requires an unspecified number of iterations to get some consistent solution – which besides may not be unique [30]. From here one gets that the order of the method is N^2 in 2D and $N^{2.5}$ in 3D; for other methods algorithms of order N can be found.

Finally, the most versatile and common approach is the standard molecular dynamics with a fixed time-step, known as time-driven molecular dynamics (TDMD). This is for many applications the slowest method, but its simplicity, applicability to different problems, and suitability for parallelization makes it the workhorse of the field. The method will be explored in the next section.

3. Time-driven molecular dynamics

The idea behind this approach is simply to integrate Newton's equations using very small time-steps, assuming that the collision between two grains is *not an instantaneous event*, but that it does represent some dynamical process that occurs over some finite interval of time, small as it may be. The main assumption is that the grains are not perfectly rigid, but that there is some elasticity and therefore some deformation upon contact. Because of this condition the method is sometimes referred to as soft particle simulations. This approach may look initially simply as an approximation, but in fact it goes to the actual physical process of a collision: in real life, there are no perfectly rigid bodies, any piece of matter deforms on a collision, and any collision takes some time to run its course. Then, in a way, TDMD is trying to be faithful to the actual physics.

In reality the implementation of TDMD requires other approximations that diminish the faithfulness, namely the definition of the interaction potential, the definition of frictional forces, and in particular the handling of static friction. There is of course the extra approximation involved in the integration method, that will be mentioned later.

3.1 *Potentials and dissipative forces*

Consider the same situation of two colliding grains, both with spherical symmetry, as was described before. We assume here that there is no force between these spherical grains when they do not touch, although it is also possible to include short-distance forces – say, some adhesion caused by liquid films on the surfaces – or even long distance potentials. The calculation of excluded-volume forces start with the compression, which is defined by

$$\xi \equiv \max(0, R_a + R_b - |\Delta \mathbf{r}|); \tag{13}$$

also of importance is the rate of change of this compression, $\dot{\xi}$. One then calculates a normal force, which can be given by many different expressions [31,32]. The simplest one, often used, assumes a linear spring with dissipation proportional to $\dot{\xi}$, and is given by

$$f_n = \min(0, -\kappa\xi - \Gamma\dot{\xi}). \tag{14}$$

This force is simple and robust, and gives in many situations results that compare quite well with experiments. The min function is included so that the force is always repulsive, and this is fundamental since the simple force $-\kappa\xi - \Gamma\dot{\xi}$ becomes positive near the end of a collision, as long as the grains separate with finite speed, when ξ is small and $\dot{\xi}$ is finite and negative. Within the restriction given in eq. (14), and using the definitions $\Omega \equiv \sqrt{\kappa/m_{\text{eff}}}$, $\gamma = \Gamma/2m_{\text{eff}}$ and $\omega = \sqrt{\Omega^2 - \gamma^2}$, where $m_{\text{eff}} = (m_a^{-1} + m_b^{-1})^{-1}$, the explicit calculation of the collision time gives [33]

$$\omega\, t_{\text{coll}} = \begin{cases} \pi - \arctan(2\gamma\omega/(\omega^2 - \gamma^2)), & \text{for} \quad \gamma < \Omega/\sqrt{2} \\ \arctan(2\gamma\omega/(\omega^2 - \gamma^2)), & \text{for} \quad \gamma > \Omega/\sqrt{2} \end{cases} \tag{15}$$

and the normal restitution constant is simply

$$\epsilon_n = \mathrm{e}^{-\gamma t_{\text{coll}}}. \tag{16}$$

Notice that here only under-damped collisions are considered. A more comprehensive discussion can be found in ref. [33].

A better approximation to the actual physics of a collision is given by the well-known Hertz formula. To include dissipation a good approach is given by [34,35]

$$f = \min(0, -\kappa_{\text{H}}\xi^{3/2} - \Gamma_{\text{H}}\xi^{1/2}\,\dot{\xi}). \tag{17}$$

This form does not allow for an analytic calculation of t_{coll} or ϵ_n, although some detailed approximations are given in [36]. Notice that in this case the second argument of the min function in (17) also represents an attractive force near the end of the collision, and the restriction to repulsive forces, instead of using the simple Hertz force $-\kappa_{\text{H}}\xi^{3/2} - \Gamma_{\text{H}}\xi^{1/2}\dot{\xi}$ for all $\xi > 0$, modifies not only the values of t_{coll} and ϵ_n, but also their qualitative dependence on the collision's parameters [36].

Although there are many other options – for instances, forces of the form $-\kappa_{\text{H}}\xi^{3/2} - \Gamma\dot{\xi}$ [37], or $-\kappa_{\text{H}}\xi^{3/2} - \Gamma\xi^{1/4}\dot{\xi}$ [38] have been explored – this section

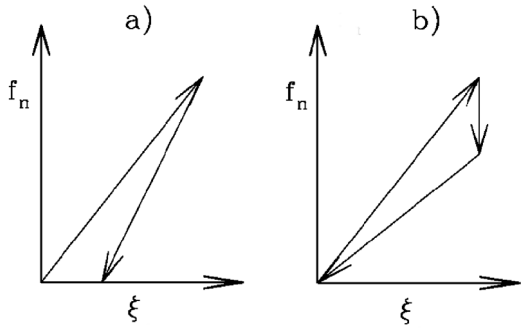

Figure 2. Two options for the force vs. compression diagram in the two-springs approach. In (**a**) some plastic deformation remains after the end of the collision.

will finish mentioning just another approach that is even simpler than the linear-spring dash-pot formula. It considers two different spring constants for loading and unloading [39]. The original version of this approach is given by the force vs. compression graph given in figure 2a, where in the unloading part of the collision the normal force vanishes for some finite compression (this is due to viscoelasticity). Another way of implementing the same idea is to reduce the value of κ during the unloading part of the collision, making in this way the dissipation simply a modification of the strength of the spring, as shown in figure 2b. In any case, the loading–unloading triangle in the diagram represents work, and that in turn is the energy lost in the collision.

3.2 *Friction and tangential forces*

The basic description of dry frictional forces between macroscopic bodies is well-known since Coulomb, but the implementation of these forces in a numerical simulation is not simple (making this issue one of the main selling points for CD). Looking only at the magnitudes, the Coulomb prescription is

$$f_{\mathrm{s}} < \mu_{\mathrm{s}} f_n \qquad \text{(static friction)}, \tag{18}$$

$$f_{\mathrm{d}} = \mu_{\mathrm{d}} f_{\mathrm{n}} \qquad \text{(dynamic friction)}, \tag{19}$$

where in general $\mu_{\mathrm{s}} > \mu_{\mathrm{d}}$, and both constants are in the (0,1) range. Dynamic friction is not too complicated to implement, since it is just proportional to normal forces, with its direction opposite to the tangential relative velocity, already given in (2). Once this direction is defined, one only needs to add a frictional component $-\mu_{\mathrm{d}} f_{\mathrm{n}} \hat{\mathbf{v}}_{\mathrm{s}}$ to the forces, and calculate the corresponding torques. In many situations this is enough to give a reasonable description of the granular medium; there are however some situations where *static* friction is fundamental: for instance, any pile of grains more than a monolayer thick and supported by a flat surface depends on static friction for its very existence.

To implement this static component an often used prescription is the Cundall–Strak form [40]; for simplicity only the 2D form (collisions between disks) of this

frictional force will be covered here. In this approach it is assumed that static friction can be represented by a stiff spring whose elongation is given by the tangential displacement ζ (of a with respect to b) accumulated from the instant of contact t_0, something that in 2D is the scalar

$$\zeta = \int_{t_0}^{t} v_{\mathrm{s}}(t')\,\mathrm{d}t'. \tag{20}$$

It is understood that this tangential spring disappears when the two disks break contact. Here v_{s} is the tangential relative velocity, given in 2D by

$$v_{\mathrm{s}} = (\mathbf{v}_a - \mathbf{v}_b)\cdot\hat{\mathbf{s}} + (R_a\omega_a + R_b\omega_b), \tag{21}$$

where $\hat{\mathbf{s}} = \hat{\mathbf{z}}\times\hat{\mathbf{n}}$, assuming dynamics confined to the x–y plane.

The tangential displacement ζ produces a force $f_{\mathrm{s}} = -\kappa_{\mathrm{s}}\zeta$, that, following Coulomb's prescription with equal friction constants, should always be smaller than the possible dynamic friction. So the final friction force is usually written as [31]

$$f_f = -\min(|\kappa_{\mathrm{s}}\zeta|, |\mu f_n|)\,\mathrm{sign}(\zeta). \tag{22}$$

A naive implementation of these equations can lead to some unphysical behavior, since long-lasting contacts may involve several changes from rolling to sliding and back, without breaking contact between the disks. This in turn can produce arbitrarily large values for ζ, since by definition it keeps on growing even when the disks are sliding. This difficulty is simply solved by controlling the growth of ζ, using [41]

$$\zeta = \int_{t_0}^{t} v_{\mathrm{s}}(t')\,\Theta\left(\mu f_n/\kappa_{\mathrm{s}} - |\zeta(t)|\right)\,\mathrm{d}t' \tag{23}$$

with the simple posterior definition of $f_f = -\kappa_{\mathrm{s}}\zeta$. Here Θ is the Heaviside function.

One final ingredient needs to be added: representing static friction with a fictitious spring has the disadvantage of introducing tangential oscillations in the system. In order to damp them one needs to put some dissipation in this tangential interaction. Following the linear-spring dash-pot model one needs to add to (22) a term of the form $-\Gamma_{\mathrm{s}}\dot{\zeta}$. For the parameter κ_{s}, ref. [31] uses the matching of the periods for compressive and tangential oscillations and give $\kappa_{\mathrm{s}}/\kappa_n = 2/7$, although reasonable results (in comparison with experiments) are found for close values, like $\kappa_{\mathrm{s}}/\kappa_n = 1/5$. For disks the same prescription gives $\kappa_{\mathrm{s}}/\kappa_n = 1/3$. The simplest option for Γ_{s} is to make it proportional to Γ_n, using the same proportional constant used for the ratio $\kappa_{\mathrm{s}}/\kappa_n$.

3.3 *Integrators*

The next step in the TDMD simulation is the actual integration of the equations of motion. There are several well-known algorithms to this, but in practice few are relevant. The basic initial point in a simulation of this kind is that the most

computationally expensive part of the process is the calculation of forces, and therefore the integration algorithm should evaluate them only once at every iteration. This leaves out some of the common workhorses in the area, like all the high-order Runge–Kutta methods.

The surviving algorithms can be roughly divided in to two camps: the Verlet and Verlet-related methods, that are symplectic in the absence of dissipation, and the Gear family of predictor–corrector formulas. A very complete description of most of these algorithms can be found in MD textbooks [16,17]. For concreteness only three among the most often used will be mentioned here: the *velocity-Verlet*, the *Beeman* and the *Gear sixth-order* algorithms.

The velocity-Verlet method advances the phase-space variables over one time-step $\mathrm{d}t$ using the formulas

$$\mathbf{r}(t+\mathrm{d}t) = \mathbf{r}(t) + \mathbf{v}(t)\,\mathrm{d}t + \mathbf{a}(t)\,\mathrm{d}t^2 + \mathcal{O}(\mathrm{d}t^3), \tag{24}$$

$$\mathbf{a}(t+\mathrm{d}t) = \mathbf{F}(\mathbf{r}(t+\mathrm{d}t))/m, \tag{25}$$

$$\mathbf{v}(t+\mathrm{d}t) = \mathbf{v}(t) + \frac{1}{2}(\mathbf{a}(t+\mathrm{d}t) + \mathbf{a}(t))\,\mathrm{d}t + \mathcal{O}(\mathrm{d}t^3). \tag{26}$$

This algorithm is *self-starting*, that is, it does not need information about the value of the variables at previous times, or the values of higher derivatives. As mentioned, it is symplectic. It is also very popular in actual use, the facility of its coding being an advantage not to be ignored. Many other options arise within this line of algorithms, some equivalent to the one just described, others with higher order precision.

However, the algorithm as given above is not correct for most applications in granular matter, where velocity-dependent forces appear. The simplest solution is to include a predictor step for the velocity, to improve the evaluation of the force in eq. (25). The resulting formulas are now

$$\mathbf{r}(t+\mathrm{d}t) = \mathbf{r}(t) + \mathbf{v}(t)\,\mathrm{d}t + \frac{1}{2}\mathbf{a}(t)\,\mathrm{d}t^2 + \mathcal{O}(\mathrm{d}t^3), \tag{27}$$

$$\mathbf{v}_p(t+\mathrm{d}t) = \mathbf{v}(t) + \mathbf{a}(t)\,\mathrm{d}t + \mathcal{O}(\mathrm{d}t^2), \tag{28}$$

$$\mathbf{a}(t+\mathrm{d}t) = \mathbf{F}(\mathbf{r}(t+\mathrm{d}t), \mathbf{v}_p(t+\mathrm{d}t))/m, \tag{29}$$

$$\mathbf{v}(t+\mathrm{d}t) = \mathbf{v}_p(t) + \frac{1}{2}\left[\mathbf{a}(t+\mathrm{d}t) - \mathbf{a}(t)\right]\,\mathrm{d}t + \mathcal{O}(\mathrm{d}t^3). \tag{30}$$

A more elaborate approach is given by the following Beeman algorithm [42,43] for velocity-dependent forces:

$$\mathbf{r}(t+\mathrm{d}t) = \mathbf{r}(t) + \mathbf{v}(t)\,\mathrm{d}t + \frac{1}{6}\left[4\,\mathbf{a}(t) - \mathbf{a}(t-\mathrm{d}t)\right]\,\mathrm{d}t^2 + \mathcal{O}(\mathrm{d}t^4), \tag{31}$$

$$\mathbf{v}_p(t+\mathrm{d}t) = \mathbf{v}(t) + \frac{1}{2}\left[3\,\mathbf{a}(t) - \mathbf{a}(t-\mathrm{d}t)\right]\mathrm{d}t + \mathcal{O}(\mathrm{d}t^3) \tag{32}$$

$$\mathbf{a}(t+\mathrm{d}t) = \mathbf{F}\left(\mathbf{r}(t+\mathrm{d}t), \mathbf{v}_p(t+\mathrm{d}t)\right)/m, \tag{33}$$

$$\mathbf{v}(t+\mathrm{d}t) = \mathbf{v}(t) + \frac{1}{12}\left[5\,\mathbf{a}(t+\mathrm{d}t) + 8\,\mathbf{a}(t) - \mathbf{a}(t-\mathrm{d}t)\right]\,\mathrm{d}t + \mathcal{O}(\mathrm{d}t^4). \tag{34}$$

It should be noticed that this algorithm is not self-starting, some other method (may be a fourth-order Runge–Kutta, or a simple Euler with a much reduced

time-step) has to be used to generate good quality values for the needed quantities at the past time $t - \mathrm{d}t$.

The second family of methods does a complete predictor–corrector calculation for all variables, and represents basically an adaptation of the Adams–Bashford–Moulton sequence of algorithms, moving the dependence on previous values of $\mathbf{r}$ and $\mathbf{v}$ to a dependence on higher derivatives. A very commonly used form [20] is the sixth-order algorithm, given as follows. Define first the following quantities:

$$\begin{aligned}
&\mathbf{V}(t) = \mathbf{v}(t)\,\mathrm{d}t, \quad \mathbf{A}(t) = \mathbf{a}(t)\,\mathrm{d}t^2, \\
&\mathbf{J}(t) = [\mathrm{d}\mathbf{a}(t)/\mathrm{d}t]\,\mathrm{d}t^3, \quad \mathbf{K}(t) = [\mathrm{d}^2\mathbf{a}(t)/\mathrm{d}t^2]\,\mathrm{d}t^4, \\
&\mathbf{L}(t) = [\mathrm{d}^3\mathbf{a}(t)/\mathrm{d}t^3]\,\mathrm{d}t^5.
\end{aligned} \tag{35}$$

Then the prediction step is a simple application of Taylor's expansion to fifth order for a well-behaved function:

$$\begin{pmatrix} \mathbf{r}_p(t+\mathrm{d}t) \\ \mathbf{V}_p(t+\mathrm{d}t) \\ \mathbf{A}_p(t+\mathrm{d}t) \\ \mathbf{J}_p(t+\mathrm{d}t) \\ \mathbf{K}_p(t+\mathrm{d}t) \\ \mathbf{L}_p(t+\mathrm{d}t) \end{pmatrix} = \begin{pmatrix} 1 & 1 & 1/2 & 1/6 & 1/24 & 1/120 \\ 0 & 1 & 1 & 1/2 & 1/6 & 1/24 \\ 0 & 0 & 1 & 1 & 1/2 & 1/6 \\ 0 & 0 & 0 & 1 & 1 & 1/2 \\ 0 & 0 & 0 & 0 & 1 & 1 \\ 0 & 0 & 0 & 0 & 0 & 1 \end{pmatrix} \begin{pmatrix} \mathbf{r}(t) \\ \mathbf{V}(t) \\ \mathbf{A}(t) \\ \mathbf{J}(t) \\ \mathbf{K}(t) \\ \mathbf{L}(t) \end{pmatrix}. \tag{36}$$

With the predicted values one evaluates now the forces, and gets the basic correction

$$\Delta\mathbf{A} = \frac{1}{2}\left[\frac{1}{m}\mathbf{F}(\mathbf{x}_p(t+\mathrm{d}t), \mathbf{v}_p(t+\mathrm{d}t))\,\mathrm{d}t^2 - \mathbf{A}_p(t+\mathrm{d}t)\right], \tag{37}$$

and from here generate the corrected quantities

$$\begin{pmatrix} \mathbf{r}(t+\mathrm{d}t) \\ \mathbf{V}(t+\mathrm{d}t) \\ \mathbf{A}(t+\mathrm{d}t) \\ \mathbf{J}(t+\mathrm{d}t) \\ \mathbf{K}(t+\mathrm{d}t) \\ \mathbf{L}(t+\mathrm{d}t) \end{pmatrix} = \begin{pmatrix} \mathbf{r}_p(t+\mathrm{d}t) \\ \mathbf{V}_p(t+\mathrm{d}t) \\ \mathbf{A}_p(t+\mathrm{d}t) \\ \mathbf{J}_p(t+\mathrm{d}t) \\ \mathbf{K}_p(t+\mathrm{d}t) \\ \mathbf{L}_p(t+\mathrm{d}t) \end{pmatrix} + \begin{pmatrix} 3/16 \\ 251/360 \\ 2 \\ 11/3 \\ 4 \\ 2 \end{pmatrix} \Delta\mathbf{A}, \tag{38}$$

with a local truncation error $\mathcal{O}(\mathrm{d}t^6)$. This theoretical accuracy may look impressive, but in reality the numerical simulations are never anywhere this good. To begin with, as has been pointed out in the standard ref. [17], MD with many-body interactions is a clear case of chaotic dynamics, and so, even assuming the unphysical (and not too interesting) situation of just one grain interacting with a fixed background of other grains, the chaotic nature of the dynamics implies a fast divergence between calculated and exact trajectories. Now, to this problem one should add the fact that in reality all grains are moving, and therefore the potential landscape in which a given grain is moving changes constantly [16]. And finally, what really spoils high-order precision in the integrators is the fact that the most often used force prescriptions between grains, eqs (14) and (17), are either discontinuous or have divergent derivatives at the moment of contact (or breaking contact), for any

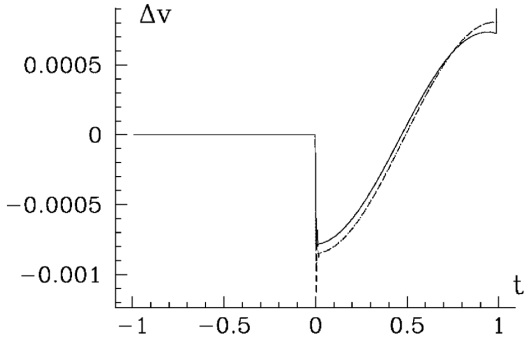

Figure 3. Difference between speeds for a numerically integrated and analytically solved collision. Here $t = 0$ has been set at contact, $t < 0$ corresponds to free flight, where all integrating algorithms become exact. For $t > 0$ the solid line gives the error for the Beeman algorithm, and the dash–dot line is a superposition of the errors for the modified velocity Verlet and the Gear sixth-order methods, that cannot be separated at the scale of the graph. The time step was set to 1/200 of half a period of the oscillation.

impact with a nonzero velocity, and this introduces a large error at contact time that usually nullifies any accuracy gained by higher-order methods.

To see how this affects the behavior of the simulations, consider the simplest possible example: a grain with some initial velocity v_0 hits a hard flat surface. Using the linear-spring dash-pot model for the force, one can get an exact integration of the collision (ignoring for simplicity the restriction to repulsive forces at the end of the collision). The dynamics can also be numerically integrated, and in figure 3 the difference between this exact solution and the modified velocity Verlet, Beeman and Gear sixth-order algorithms are shown. It is clear from the figure that there is almost no difference in the accuracies of these three integrators, and that the largest error comes from the discontinuities at the moment of contact.

4. Example: The discharge of a 2D silo

The discharge of granular matter from a container is a very common phenomenon, but it is not yet completely understood. In practice, one has only a few empirical rules to explain the process [6,44,45]. Due to its intrinsic interest and its obvious practical applications this phenomenon has received much attention recently.

A common example of granular matter discharge is given in hoppers and silos [46]. In these containers jamming – that is, a complete arrest of the flow making the granular material behave like a solid – is known to appear as soon as the size of the exit hole is reduced to a few times the average diameter of the grains inside. Experimental work in both 2D and 3D hoppers [47,48] and silos [49–53] have shown that jamming depends only on the ratio between particle and exit hole sizes, as long as the diameter and height of the silo are large enough such that (1) the boundary effects of the walls can be neglected and (2) the pressure at the bottom of the silo saturates, following the Janssen effect [6].

A question not yet fully answered about silos, and one of the simplest and more fundamental, is the possible existence of a critical hole size such that for larger holes the flow cannot jam. This critical size has been found to exist in experiments for several types of grains, such as smooth and rough spheres and edible grains [50]. The same work shows that the distribution of avalanche sizes for a given value of R can be well fitted to an exponential, and this in turn is consistent with a simple model where each grain – may be cluster of grains – has a constant probability of exiting the silo, uncorrelated to the behavior of other grains (clusters).

However, experiments carried in 2D [47,48], although supporting the hypothesis of a fixed probability of exiting the silo for each grain, point towards a probability of jamming that is exponentially decaying on R^2. The earlier work reported in [52] supports the hypothesis of an exponential divergence in R for the average avalanche.

The difference between both types of behavior is of a fundamental type: in the second case grains flowing out of a silo is a transitory phenomenon, since there is always a non-zero – even if exponentially small – probability of jamming. In the first case one gets an assurance that for large enough holes the flow will never develop a spontaneous blockage, and it is then a truly stationary process.

Here, as an example of the uses of numerical techniques in the study of granular matter, a simulation of a 2D silo with variable hole size is given. This simulation tries to get some information on the statistics of its discharge, and on the possible presence of criticality in this process. There are some obvious limitations to this particular simulation that puts it at a disadvantage with respect to actual experiments, chiefly the fact that tracking the very long avalanches that appear for large exit hole sizes consume an inordinate amount of computer time. Still, a systematic study of the avalanches for different exit hole sizes allows the identification of some well-defined trends.

Some previous simulations on the flow and jamming of silos were carried out in [54] and [55]. In the later work the flow was simulated using a highly simplified dynamics, built on inertia-less vertical and rolling movements applied sequentially to the grains in the silo. The avalanches found for this model were distributed as a power-law (becoming then an example of self-organized criticality [56]), while the divergence of the average avalanche as a function of the exit hole size was inferred to be an exponential in R.

4.1 *Simulation*

The simulations were done over an ensemble of N polydisperse disks, with diameter given by $d_i = d_{\text{ave}} + x\Delta d$, where d_{ave} is the average diameter, Δd is its maximum fluctuation, and x is randomly chosen from the $[-1, 1]$ uniform distribution. Polydispersity is used here to frustrate the formation of crystalline (hexagonal) domains. The silo has a bottom size D and indefinite height. At the center of the bottom there is a hole of size d_{h}. The disks have a 2D mass density σ, and the gravitational acceleration g acts in the negative y direction. Upon contact, the disks interact with the (perfectly rigid) walls of the silo, and with each other, via a linear spring with a constant that on loading has the value κ, and on unloading is reduced by a restitution factor ϵ^2. The interaction is complemented by dynamic and static

friction, using for both the same coefficient μ. Equations of motion were integrated using the modified velocity-Verlet algorithm reported before.

It is possible to use natural units where the disks' average diameter and mass, together with the gravitational constant, are set to one, fixing in this way length, mass and time scales. Here the numerical experiment has been implemented with standard units, and have used $N = 2000$ disks with $d_{\mathrm{ave}} = 0.5$, $\Delta d = 0.05$, $D = 15$, $\sigma = 0.8$ and $\kappa = 4 \times 10^6$, with all quantities given in the cgs system. This value for κ is not as large as could be expected for some hard real systems (steel or glass spheres, for instance), but it allows for a more efficient use of computer time. It can be realistic enough for softer grains, like the rice or lentils used in [50]. It has also been reported that changes of up to one or two orders of magnitude in the stiffness of the grains have little influence on the results of these types of simulations [57]. A warning should be given, however, about the use of very soft grains in these numerical calculations: there are in this case two well-characterized deficiencies in the simulation: *brake failure*, where in glancing collisions one does not find the correct scaling for the reduction of the tangential velocity, and *detachment effect* where a large number of grains in a compact cluster starts behaving as a single elastic solid, failing to display the multiple intergranular collisions responsible for the fast dissipation of energy [29,31]. The adimensional quantities μ and ϵ^2 have been set at 0.5 and 0.9 respectively. Gravity is fixed as $g = 981$. The ratio between the diameters of the disks and the silo gives $D/d_{\mathrm{ave}} = 30$, and for the number of disks used the silo gets filled up to a height of around 2.5 times D. These two values are large enough to put the silo in the limit where both the effects of the walls and the height of the load become irrelevant [49,50,58], at least for the 3D case. A time-step of 0.01 times the disk–disk collision time t_{coll} was used. For later convenience, the time and speed scales $t_0 = \sqrt{d_{\mathrm{ave}}/g}$ and $v_0 = g\, t_0$ are also defined.

The simulation proceeds as follows: first the silo is closed from below and the disks are placed in a regular grid with random initial velocities. The system is then allowed to relax, under the influence of gravity, up to the moment where the maximum speed detected is some small fraction of v_0. At this point a hole of length d_{h} appears at the center of the bottom line, and disks start pouring out of the silo. These falling disks are followed until their centers are a distance $\approx 1.3 d_{\mathrm{ave}}$ below the bottom, and at this moment they are eliminated from the exiting flow and re-injected on top of the system, at a distance of $5.5\, d_{\mathrm{ave}}$ from the surface of the dense aggregate of disks. In re-injection the disks preserve their z velocity, but their horizontal velocity is set to zero. The re-injection point is chosen so as to keep the top of the material roughly flat. With these conditions the observed flow is of a mixed type, neither massic nor funnel-like; the disks close to the center of the silo fall faster than those close to the walls, but the speed difference is not too large.

Occasionally, an arch is formed above the exiting hole and the flow stops. Given that static friction is included, these arcs are not always convex. This jammed state is detected by checking that (1) the *maximum* speed in the system is less than v_0/c and (2) no disk has exited the silo in a time longer than $c\, t_0$. It has been found that for the purposes of this simulation $c = 8$ is adequate. One needs to be aware that, due to numerical truncation, the maximum velocity during a jamming event does not decay all the way to zero, but saturates. (For the parameters used here, this velocity saturates to a small value close to $v_0/160$.) This persistent vibrational

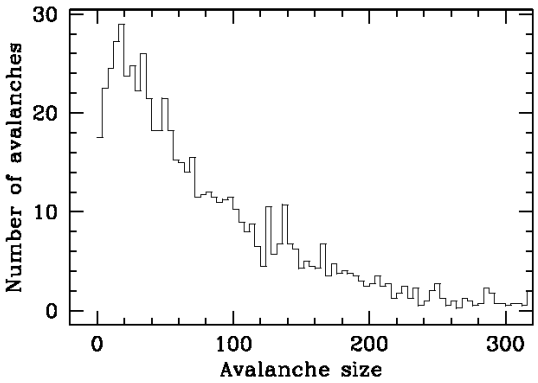

Figure 4. Histogram of avalanches for $R = 3.6$. Bin size has been set to 4, and null avalanches have not been included.

noise implies that the actual succession of avalanches does depend on c, but as mentioned, without affecting the statistics.

Once the two conditions that mark a jamming are fulfilled, the silo receives a tap given by vertical displacement $z_{\text{tap}} = A\sin(2\pi\nu t)$, applied for half a period. Here $A = 0.6$ and $\nu = 8.0$ have been used. In most cases this tap is enough to break the arch or arches that are blocking the flow; however, given that the tap moves the whole material in parallel, it does occasionally happen that there is not enough rearrangement of the disks to break the blockage. It is possible therefore with this unjamming protocol to get *null avalanches*, which are time intervals between two taps where no material flows out of the silo. These null avalanches are highly correlated among themselves, in the sense that, for small openings, they tend to appear next to each other in the time record. This type of events have also appeared in the experiments reported by Zuriguel [59]. Null avalanches are common for very small hole sizes, less so for larger openings.

4.2 *Results*

The simulation has been carried on for hole sizes from 1.70 to 2.25, in steps of 0.05, corresponding to hole/particle ratios R from 3.4 to 4.5 in steps of 0.1. In all cases several runs starting from different grain configurations have been performed. For each size at least 1000 avalanches are obtained. For all R values the distributions of avalanches $n(s)$ show basically an exponential form, except for a spike at $s = 0$ (null avalanches), and a weak dip for small s (see figure 4). These two characteristics are probably a peculiarity of the method used here to unjam the silo. It should be noticed that the decrease in $n(s)$ found for small s is not as pronounced as the one reported from the experiments [50]. As for the probability of finding null avalanches, it goes from a maximum of 0.20 at $R = 3.4$ to a minimum of 0.019 at $R = 4.4$, but there is not enough statistics as to be able to predict their presence or absence for larger values of R.

To avoid having to fix a bin size in the histograms, the normalized cumulative distribution is used:

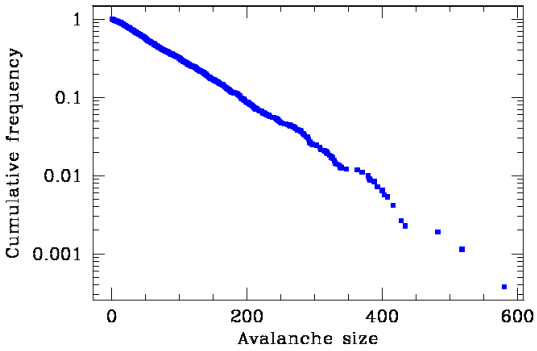

Figure 5. Cumulative curve $w(s)$ for $R = 3.6$. Null avalanches are excluded.

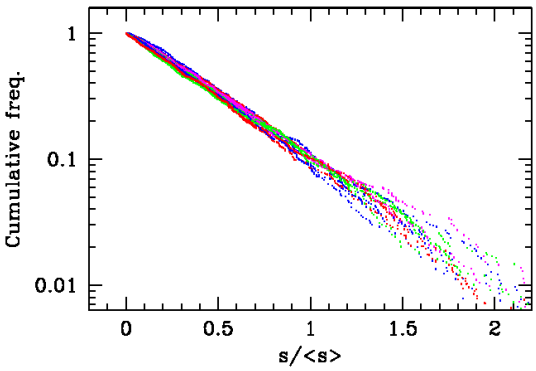

Figure 6. Collapse of the cumulatives $w(s)$ for all values of R considered. The regions of non-exponential behavior found for small s have some incidence over the observed dispersion, since in all cases the normalization is $w(1) = 1$. The values of the average avalanche vary from $\langle s\rangle = 50.4$ for $R = 3.4$ to $\langle s\rangle = 1385.3$ for $R = 4.5$.

$$w(s) = \sum_{s'=s}^{\infty} n(s') / \sum_{s'=1}^{\infty} n(s'), \tag{39}$$

that is, one counts the number of avalanches with s or more disks. Notice that in this measure the null avalanches are left out. For a properly normalized exponential distribution the normalized cumulative happens to be identical to the distribution itself. Figure 5 shows the cumulative avalanche distribution for $R = 3.6$. Given the claim that the distribution is exponential for all cases, it should be possible to scale s to obtain a collapse of all cumulatives. This is shown in figure 6. Even so, it should be remembered that the distribution is not a perfect exponential, due to the smaller probabilities found for very small avalanches. This effect is almost imperceptible in the cumulatives.

The question that remains to discuss is the behavior of the average avalanche $\langle s\rangle$ with respect to the hole/particle ratio. As expected, a rapidly growing curve is found. In logarithmic scale a faster than linear behavior is found, and so an

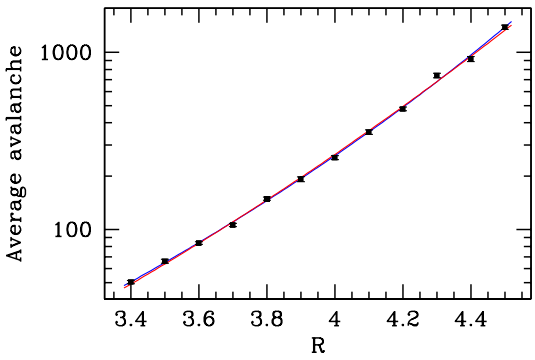

Figure 7. Scaling of the average avalanche $\langle s \rangle$ against the exit-hole/disk ratio R. Both the power-law fit and the exponential-square fit are shown (with parameters given in the text). At the scale of the figure both lines superpose almost perfectly.

exponential divergence of the form $\langle s(R) \rangle \approx s_0 \exp(AR)$ may be discarded. However, it is also clear from the figure that an exponential divergence in some higher power of R (or even some polynomial in R) cannot be ruled out. In particular, the form $\langle s(R) \rangle \approx s_0 \exp(BR^2)$ proposed in [48] should be considered. Another option is a power-law of the form $\langle s(R) \rangle \approx s_0/(R_c - R)^\gamma$.

Trying both expressions for the results of this simulation, it is found that the the avalanche averages give similar quality fits for either the exponential-of-square or the power-law formulas, as can be seen in figure 7. For the first expression the parameters $s_0 = 1.64 \pm 0.08$ and $B = 0.0716 \pm 0.0006$ are found, with $\xi^2 = 0.20$. In the second case the fit gives $s_0 = 8.5 \times 10^5$, $R_c = 6.7 \pm 0.4$ and $\gamma = 8.2 \pm 1.1$. For this fit the χ^2/dof is 0.17. It is then clear that with the available data the difference between the two fits is not really large enough as to allow for a definite conclusion, as can be well seen in the figure, where the two behaviors superpose almost perfectly.

Moreover, some other types of divergence have been hinted at, like an essential singularity given by $\langle s \rangle \approx s_0 \exp[1/(R_c - R)]$. Still, the results agree with the most extensive experiments performed at this time, and therefore adds support to the existence of criticality in the jamming of silos. This leaves open the more fundamental question about the origin of the correlations that may lead to critical behavior in this type of phenomena.

So, the bottom line for simulations is at the moment mixed: on one side, the general exponential form of the avalanche distribution for a given R is well confirmed, together with some other details like the deviation from this exponential for small avalanches, and even the existence of null avalanches [59]. Unfortunately, the simulations cannot get close enough to the proposed critical regime as to be able to either confirm or deny it; the simple $\exp(BR^2)$ regime proposed as an alternative is also found to be compatible with the data. This is not the case for the published data in the 3D experiments [50]: there, a fit to an exponential clearly fails. One then has two options: either the behavior for the avalanches in 2D is also critical, and neither experiments nor simulation have reached the correct regime, or there is

a fundamental difference between the 3D and the 2D behaviors, one being critical while the other is not. There is also, up to now, no indication at all of what physical mechanisms may be responsible for criticality; or in other words, why stable arches above certain size are impossible to generate. Naively, one would think that the chance appearance of large arch is simply a very rare event, not an impossibility.

Besides the obvious – but computationally difficult – option of moving to larger values of R, there are other tests that may be applied to the data generated by this type of simulations in order to see if there is any sign of criticality. In particular, it is of interest to analyze different time series that the simulation generates, like the time intervals between grains leaving the silo, or the time evolution of average and maximal stress. This work is now in progress.

5. Conclusions and final comments

This work has tried to give a view – incomplete and very basic – of how to do numerical simulations in granular matter, concentrated in the few techniques that are more frequently used. The very fundamental issue of parallelization is left out, as are some interesting approximations that fall outside the molecular dynamics camp, as are some types of cellular automata. Left out are also the extensions needed for the description of non-spherical grains.

As mentioned, the three broad categories of algorithms considered here have different areas of application: for instance, very dense flows with a static final configuration and almost null restitution coefficient – a landslide is a good example – are well suited to a CD simulation, while a diluted and almost elastic gas falls more into the domain of EDMD. Still, there are no absolute limits among the applicability ranges of the different algorithms, and in practice the availability of the codes and the know-how developed over years of practice are paramount in the researchers' choice. In any simulation there will be some trade-offs, but it is still comforting to see that qualitative – and often also quantitative – features of granular flows are well described by the simulations.

The fundamental problem of the approximations in the definition of forces is something that should not be completely ignored: for TDMD the force definitions assume a clean split between compressional and frictional stresses, employs very simplified models for frictional effects, and even the realistic Hertz forces [34,35] are in part extrapolated from the static limit. One should probably wait for more experiments, and for the very detailed numerical exploration of the collision of just two grains, for models that can be closer to reality and applicable under broader conditions. The price that will be paid of course is the increase in computational complexity that those models will imply.

References

[1] J Duran, *Sands, powders and grains* (Springer, New York, 2000)
[2] H M Jaeger and S R Nagel, *Rev. Mod. Phys.* **68**, 1259 (1996)
[3] P G de Gennes, *Rev. Mod. Phys.* **71**, S374 (1999)
[4] J Kakalios, *Am. J. Phys.* **73**, 8 (2005)

[5] I Zuriguel, T Mullin and J M Rotter, *Phys. Rev. Lett.* **98**, 028001 (2007)
[6] H A Janssen, *Z. Ver. Dtsch. Ing.* **39**, 1045 (1895); translated to English by M Sperl in arXiv:cond-mat/0511618v1
[7] A J Liu and S R Nagel, *Nature (London)* **396**, 21 (1998)
[8] A Rosato, K J Strandburg, F Prinz and R H Swendsen, *Phys. Rev. Lett.* **58**, 1038 (1987)
[9] R Jullien, P Meakin and A Pavlovitch, *Phys. Rev. Lett.* **69**, 640 (1992)
[10] T Schnautz, R Brito, C A Kruelle and I Rehberg, *Phys. Rev. Lett.* **95**, 028001 (2005)
[11] M P Ciammarra *et al*, *Phys. Rev. Lett.* **96**, 058001 (2006)
[12] J S Olafsen and J S Urbach, *Phys. Rev. Lett.* **81**, 4369 (1998)
[13] J S Olafsen and J S Urbach, *Phys. Rev.* **E60**, R2468 (1999)
[14] X Nie, E Ben-Haim and S Y Chen, *Europhys. Lett.* **51**, 679 (2000)
[15] N V Brilliantov and T Pöschel, *Kinetic theory of granular gases* (Oxford Univ. Press, Oxford, 2004)
[16] M P Allen and D J Tildesley, *Computer simulation of liquids* (Oxford Univ. Press, Oxford, 1987)
[17] D Frenkel and B Smit, *Undersatanding molecular simulation: From algorithms to applications* (Academic Press, San Diego, 2002)
[18] B J Adler and T E Wainwright, *J. Chem. Phys.* **27**, 1208 (1957)
[19] N V Brilliantov, T Pöschel, W T Kranz and A Zippelius, *Phys. Rev. Lett.* **98**, 128001 (2007)
[20] T Pöschel and T Schwager, *Computational granular dynamics* (Springer, Berlin, 2005)
[21] S McNamara and W R Young, *Phys. Fluids* **A4**, 496 (1992)
[22] S McNamara and W R Young, *Phys. Rev.* **E50**, R28 (1994)
[23] D C Rapaport, *J. Comp. Phys.* **34**, 184 (1980)
[24] D C Rapaport, *The art of molecular dynamics simulation* (Cambridge Univ. Press, Cambridge, 1995)
[25] M Marin, D Risso and P Cordero, *J. Comp. Phys.* **109**, 306 (1993)
[26] J J Moreau, *Eur. J. Mech. A-Solids* **13**, 93 (1994)
[27] M Jean, *Comput. Methods Appl. Mech. Engg.* **177**, 235 (1994)
[28] T Unger and J Kertész, in *Modeling complex systems: Seventh Granada lectures* edited by P L Garrido and J Marro (AIP, New York, 2003)
[29] D E Wolf, in *Computational Condensed Mater Physics: Lecture Manuscripts of the 37th Spring School of the Institute of Solid State Research* (IFF Ferienkurs, Forschungszentrum Jülich, 2006) vol. 32
[30] J J Moreau, in *Nonsmooth/Nonconvex Mechanics with Applications in Engineering, II. NNMAE 2006* edited by C C Baniotopoulos (Ziti, Thessaloniki, 2006)
[31] J Schäfer, S Dippel and D E Wolf, *J. Phys. I France* **6**, 5 (1996)
[32] H Kruggel-Emden *et al*, *Powder Tech.* **171**, 157 (2007)
[33] T Schwager and T Pöschel, *Granular Matter* **9**, 465 (2007)
[34] N V Brilliantov, F Spahn, J-M Hertzsch and T Pöschel, *Phys. Rev.* **E53**, 5382 (1996)
[35] G Kuwabara and K Kono, *Jpn. J. Appl. Phys.* **26**, 1230 (1987)
[36] T Schwager and T Pöschel, arXiv:cond-mat/07081434 (2007)
[37] J Lee and H J Herrmann, *J. Phys.* **A26**, 373 (1993)
[38] T Tsuji, T Tanaka and T Ishida, *Powder Tech.* **71**, 239 (1992)
[39] O R Walton and R L Brown, *J. Rheol.* **30**, 949 (1986)
[40] P A Cundall and O D L Strack, *Géotechnique* **29**, 47 (1979)
[41] L Brendel and S Dippel, *Physics of dry granular materials*, NATO ASI Series E (1998) vol. 350, p. 313
[42] D Beeman, *J. Comput. Phys.* **20**, 130 (1976)

[43] K Refson and S Pawley, *Mol. Phys.* **61**, 669 (1987)
[44] W A Beverloo, H A Leniger and J van de Velde, *Chem. Eng. Sci.* **15**, 260 (1961)
[45] R M Nedderman, U Tüzün, S B Savage and G T Houlsby, *Chem. Eng. Sci.* **37**, 1597 (1982)
[46] Here a silo is any hopper with a flat bottom
[47] K To, P Y Lai and H K Pak, *Phys. Rev. Lett.* **86**, 71 (2001)
[48] K To, *Phys. Rev.* **E71**, 060301(R) (2005)
[49] I Zuriguel, L A Pugnaloni, A Garcimartín and D Maza, *Phys. Rev.* **E68**, 030301(R) (2003)
[50] I Zuriguel *et al*, *Phys. Rev.* **E71**, 051303 (2005)
[51] M Hou *et al*, *Phys. Rev. Lett.* **91**, 204301 (2003)
[52] E Clément *et al*, *Traffic and granular flow '99* edited by D Helbing, H J Herrmann, M Schreckenberg and D E Wolf (Springer, Berlin, 2000)
[53] J Zhong, M Hou, Q Shi and K Lu, *J. Phys.: Condens. Matter* **18**, 2789 (2006)
[54] G H Ristow and H J Herrmann, *Phys. Rev.* **E50**, R5 (1994)
[55] S S Manna and H J Herrmann, *Eur. Phys. J.* **E1**, 341 (2000)
[56] P Bak, C Tang and K Wiesenfeld, *Phys. Rev. Lett.* **59**, 381 (1987)
[57] L E Silbert *et al*, *Phys. Rev.* **E64**, 051302 (2001)
[58] D Hirschfeld and D C Rapaport, *Eur. Phys. J.* **E4**, 193 (2001)
[59] I Zuriguel, Ph.D. Thesis (Universidad de Navarra, 2005) (in Spanish)